

### **OPEN ACCESS**

EDITED BY
Giorgio Treglia,
Ente Ospedaliero Cantonale (EOC),
Switzerland

REVIEWED BY Alfred Otoe Ankrah, Korle Bu Teaching Hospital, Ghana Yanni Jia, Shanxi Medical University, China

\*CORRESPONDENCE
Xuemei Wang

☑ wangxuemei201010@163.com
Dan Li

☑ 13739298619@163.com

†These authors share last authorship

RECEIVED 18 June 2025 ACCEPTED 18 August 2025 PUBLISHED 01 September 2025

### CITATION

Wen R, Xie Q, Pan B, Ni M, Zhu X, Meng X, Wei Z, Wu X, Li D and Wang X (2025) Simultaneous <sup>13</sup>N-ammonia and gadolinium perfusion using integrated PET-MRI: diagnostic accuracy in coronary microvascular dysfunction. *Front. Med.* 12:1649175. doi: 10.3389/fmed.2025.1649175

### COPYRIGHT

© 2025 Wen, Xie, Pan, Ni, Zhu, Meng, Wei, Wu, Li and Wang. This is an open-access article distributed under the terms of the Creative Commons Attribution License (CC BY). The use, distribution or reproduction in other forums is permitted, provided the original author(s) and the copyright owner(s) are credited and that the original publication in this journal is cited, in accordance with accepted academic practice. No use, distribution or reproduction is permitted which does not comply with these terms.

# Simultaneous <sup>13</sup>N-ammonia and gadolinium perfusion using integrated PET-MRI: diagnostic accuracy in coronary microvascular dysfunction

Runze Wen<sup>1</sup>, Qiang Xie<sup>1</sup>, Bo Pan<sup>1</sup>, Ming Ni<sup>1</sup>, Xingxing Zhu<sup>1</sup>, Xueer Meng<sup>1</sup>, Zhenheng Wei<sup>2</sup>, Xinai Wu<sup>2</sup>, Dan Li<sup>3\*†</sup> and Xuemei Wang<sup>1\*†</sup>

<sup>1</sup>Department of Nuclear Medicine, First Affiliated Hospital of USTC, Division of Life Sciences and Medicine, University of Science and Technology of China, Hefei, Anhui, China, <sup>2</sup>Department of Nuclear Medicine, Affiliated Hospital of Inner Mongolia Medical University, Hohhot, Inner Mongolia, China, <sup>3</sup>Department of Cardiovascular Medicine, First Affiliated Hospital of USTC, Division of Life Sciences and Medicine, University of Science and Technology of China, Hefei, Anhui, China

**Objective:** Absolute quantification of myocardial perfusion and coronary flow reserve (CFR) with positron emission tomography (PET) has demonstrated diagnostic and prognostic value in patients with coronary microvascular dysfunction (CMD). However, no studies have compared magnetic resonance imaging (MRI) and PET perfusion imaging in patients with CMD using integrated PET-MRI imaging. The aim of this study was to assess the quantitative accuracy of cardiac perfusion measurements using MRI with simultaneous <sup>13</sup>N-ammonia PET as reference with a fully integrated PET-MRI scanner.

**Methods:** Thirty patients with suspected CMD underwent simultaneous MRI and <sup>13</sup>N-ammonia PET scans at rest and regadenoson-stress on an integrated PET-MRI scanner. Correlation and agreement between MRI-and PET-derived myocardial blood flow (MBF) and CFR values were evaluated using correlation and Bland–Altman analysis.

**Results:** MRI measurements of global rest and stress MBF showed moderate correlation to those obtained using  $^{13}$ N-ammonia PET (r=0.50; p=0.005 for rest MBF and r=0.49; p<0.006 for stress MBF). Bland–Altman analysis revealed a mean bias of  $-0.83\pm0.47$  mL/g/min for rest MBF and  $-1.84\pm0.57$  mL/g/min for stress MBF. The correlations between regional MBF<sub>MRI</sub> and MBF<sub>PET</sub> obtained during rest and stress were only poor to moderate (r=0.26 and r=0.43). The limits of agreement were wide for both global and regional MBF, with larger variability for high MBF-values. However, there was good agreement between MRI and PET with regard to global and regional CFR with moderate to strong correlation (r=0.64, p<0.001; r=0.48, p<0.001). MRI-derived CFR demonstrated an area under the curve (AUC) of 0.85 (95% CI: 0.67 to 0.95) and had an optimal cutoff value of 1.57 for detecting CMD, defined as  $^{13}$ N-ammonia PET-derived CFR  $\leq 2.0$ .

**Conclusion:** CFR measurements were concordant between MRI and  $^{13}$ N-ammonia PET. For detecting significant CMD, CFR<sub>MRI</sub> and CFR<sub>PET</sub> demonstrated comparable and high accuracy. Nevertheless, MRI measurements of rest and stress MBF showed only poor to modest agreement to those obtained

with <sup>13</sup>N-ammonia PET. Therefore, although quantitative MRI has clinical utility, further refinements are still required.

KEYWORDS

myocardial perfusion, myocardial blood flow, magnetic resonance imaging, positron emission tomography, coronary flow reserve

# 1 Introduction

Microvascular disease (MVD), or coronary microvascular dysfunction (CMD) is receiving increasingly attention as 20 to 80% of patients with stable angina have normal or nonobstructive coronary artery disease (NOCAD) on coronary angiography (CAG) and coronary computed tomography angiography (CCTA) (1). Current evidence suggests that CMD is multifactorial, resulting from both impaired vasodilation of the myocardial microcirculation and an increased response to vasoconstrictive stimuli (2). Consequently, the coronary microcirculation fails to vasodilate for maintaining normal myocardial perfusion (3).

With the growing recognition that CMD represents a potential therapeutic target, accurate diagnosis of this condition has taken on greater significance. However, the diagnosis of CMD has traditionally been ascertained by means of invasive physiological assessment during angiography but this method requires an invasive pressure measurement and thus carries increased risk to patients compared to noninvasive imaging (4). In recent years, there has been increasing interest in using non-invasive modalities, including positron emission tomography (PET), to assess coronary flow reserve (CFR) as the primary criterion for CMD (5). PET provides a non-invasive method to diagnose CMD through absolute quantification of hyperemic myocardial blood flow (MBF, mL/min/g) and CFR. Reductions in these parameters provide important diagnostic and prognostic information (6). However, the use of PET involves ionizing radiation exposure, which poses challenges for routine follow-up assessments.

In clinical routine and in large clinical studies, first-pass cardiac magnetic resonance imaging (MRI) has become a clinical standard approach to assess myocardial perfusion (7–9). Derived from time-intensity or contrast concentration curves obtained from the left ventricle (LV) tissue and blood pool, the myocardial perfusion reserve index (MPRI) serves as a reliable semiquantitative imaging marker reflecting the vasodilatory capacity of the microvasculature (10). Despite its promise, this technique still lacks clinical validation against an independent reference standard.

Previous studies showed good agreement between PET and cardiac magnetic resonance imaging (CMR) for myocardial perfusion reserve (stress-to-rest MBF ratio) (11, 12). Nevertheless, numerous studies comparing MBF and/or CFR between CMR and PET have primarily focused on separate assessments of these modalities performed on common groups of subjects but separated in time and thus being subject to intrasubject variation (11, 13, 14).

Therefore, the aim of this study was to evaluate the agreement between CMR and <sup>13</sup>N-ammonia PET perfusion measurements using integrated PET-MRI imaging in a relatively large cohort of patients with CMD.

# 2 Methods

# 2.1 Study population

Data of this single-center study were derived from ongoing PET-MRI research projects. Thirty patients with suspected CMD were prospectively enrolled between September 2024 and March 2025 and examined at the first affiliated hospital of University of Science and Technology (USTC). The selection of CCTA or invasive coronary angiography was determined by cardiologists based on patient symptoms and coronary risk factors. Inclusion criteria for CMD included: (1) symptoms of myocardial ischemia and (2) non-obstructive coronary arteries (defined as <50% stenosis diameter). Exclusion criteria included: (1) presence of myocardial scar on late gadolinium enhancement (LGE), (2) history of coronary revascularization (including percutaneous coronary intervention or coronary artery bypass graft), (3) acute myocardial infarction, (4) atrial fibrillation, (5) severe valvular heart disease, (6) heart failure, (7) cardiomyopathy, (8) chronic kidney disease (eGFR < 45 mL/min), and (9) contraindications to intravenous regadenoson or CMR. All participants were specifically advised to avoid caffeine for 24 h before imaging. Ethics approval was obtained from the Ethics Committee of The First Affiliated Hospital of USTC of China for study procedures, and written informed consent was obtained from all participants prior to participation.

### 2.2 Cardiac PET-MRI protocol

All participants underwent an overnight fast of at least 6 h, except for water intake. PET-MRI scans were acquired on a 3.0 T PET-MRI system (Biograph mMR, Siemens Healthineers, Erlangen, Germany). Each patient underwent simultaneous <sup>13</sup>N-ammonia PET and gadoterate dimeglumine (Gd-DTPA) perfusion MRI scans at rest and during regadenoson-induced hyperemia.

All patients performed the rest imaging first, followed by stress imaging approximately 1 h later. For rest PET-MRI imaging, a 10 min dynamic PET perfusion scan during rest was started simultaneously with the administration of 370–555 MBq of <sup>13</sup>N-ammonia (using a second intravenous cannula) followed by a bolus of saline (20 mL at 3 mL/s). MRI perfusion imaging was conducted concurrently with the PET scan. After the start of the PET scan, a single bolus of Gd-DTPA contrast agent (Beilu Pharmaceutical, Beijing, China) (0.075 mmol/kg body weight) was administered via a power injector at a flow rate of 4 mL/s into an antecubital vein, immediately followed by a 20 mL normal saline flush. A saturation recovery turboFLASH CMR sequence was used for MRI perfusion imaging using electrocardiography (ECG)-triggered and breath holding technique. Key parameters included: TR/TE = 2.67/1.15 ms, flip angle of 20°,

field of view (FOV) =  $380 \times 304$  mm, slice thickness = 8 mm, matrix size  $128 \times 102$ , and a pre-pulse delay of 100 msec.

Stress imaging employed identical parameters to the rest perfusion sequence described above, except that regadenoson was administered 60–90 s prior to simultaneous intravenous injections of  $^{13}N$ -ammonia and Gd-DTPA. Regadenoson (400 µg) was administered via an antecubital cannula as a single intravenous bolus over less than 10 s, immediately followed by 5 mL saline flush. Dynamic PET images were reconstructed using a three-dimensional ordered-subset estimation-maximization (3D-OSEM) with 6 iterations and a 5 mm post-reconstruction filter. The dynamic frame protocol included  $12\times10$  s,  $2\times30$  s,  $4\times60$  s and  $1\times180$  s intervals using the two-point Dixon attenuation correction.

# 2.3 Image analysis

Left ventricular myocardial perfusion analysis was performed using the standardized 16-segment model defined by the American Heart Association (15). Myocardial blood flow was quantified for both the entire left ventricle and three myocardial regions corresponding to the coronary artery territories (LAD, left anterior descending; LCX, left circumflex artery; and RCA, right coronary artery). CFR was calculated as the stress-to-rest MBF ratio and analyzed at both global and regional levels, respectively.

Image analysis was independently performed by two reviewers. If there was a disagreement between the two, a third observer joined the evaluation. The final result was determined by consensus among all three. Interobserver agreement for image analysis was assessed using kappa coefficient for categorical variables and intraclass correlation coefficient (ICC) for continuous variables. A kappa value >0.75 and ICC > 0.80 were considered to indicate excellent agreement. Regions of interest were defined in the MRI images using CVI42 post-processing software (version 5.1.1, Calgary, Canada). Endocardial and epicardial contours of the left ventricle were manually traced to derive rest and stress data, with subsequent generation of time-signal intensity curves for myocardial tissue and cardiac blood pool. Concordance between CMR and PET was evaluated on a per-vessel basis.

All PET data were quantified semi-automatically using a commercially available dedicated software package (Syngo MBF®, Siemens Healthcare, Erlangen, Germany), generating MBF-values for the entire left ventricle and in three regions corresponding to the coronary artery territories. Mean CFR was calculated as the ratio of stress MBF (stress scan) to rest MBF (rest scan) in each region and globally.

### 2.4 Statistical analysis

Continuous variables were expressed as mean ± standard deviation (SD) or median with interquartile range (IQR). Categorical variables were expressed as frequency with percentage. Pearson's correlation was used to quantify association between continuous variables. Bland–Altman analysis was performed to evaluate the agreement between CMR and PET. Diagnostic performance of CMR indices for detecting CMD was evaluated through receiver-operating characteristic (ROC) curve analysis. Statistical analyses were conducted using the IBM SPSS Statistics v26.0 (SPSS Inc., Chicago,

IL), GraphPad Prism v9.0 (GraphPad Software, La Jolla CA), and MedCalc v19.1 (MedCalc Software, Ostend, Belgium). For all analyses, a two-tailed *p*-value < 0.05 was considered significant.

### 3 Results

### 3.1 Baseline characteristics

Baseline characteristics and hemodynamic parameters of the cohort of 30 patients (11 were classified as CMD and 19 as the reference group with preserved CFR) are summarized in Tables 1, 2, respectively. The protocol for the study is illustrated in Figure 1.

Although sex, BMI, and age did not differ significantly between the two study groups, patients with impaired CFR tended to be older and had higher BMI values compared to those with preserved CFR. The study group had a higher incidence of diabetes, hypertension, and hyperlipidemia than the control subjects.

# 3.2 Global myocardial perfusion

Figure 2 shows the relationship between MRI and PET measurements of global myocardial perfusion. On a per patient basis, MRI-derived CFR (CFR<sub>MRI</sub>) and PET-derived CFR (CFR<sub>PET</sub>) showed moderate correlation (r=0.64; p<0.001) and moderate inter-method reliability (ICC for absolute agreement = 0.66 [95% confidence interval (CI): 0.28 to 0.84]; p=0.003). Bland–Altman analysis demonstrated a mean bias of  $-0.79\pm0.85$  for CFR. Table 2 (the second to last row) displays the mean values of global CFR as measured using MRI and PET. Global CFR was significantly lower for MRI in comparison to PET (1.77  $\pm$  0.49 vs. 2.56  $\pm$  1.08; p<0.001). MRI-derived MBF (MBF<sub>MRI</sub>) and PET-derived MBF (MBF<sub>PET</sub>) obtained during rest and stress showed correlation (r=0.50, p=0.005 and r=0.49, p=0.006, respectively). Bland–Altman analysis demonstrated a mean bias of  $-0.83\pm0.47$  mL/g/min and  $-1.84\pm0.57$  mL/g/min for rest and stress MBF, respectively.

# 3.3 Regional myocardial perfusion

The relationship between MRI and PET measurements of regional myocardial perfusion is illustrated in Figure 3. On a per vessel basis, correlation (r = 0.48; p < 0.001) and inter-method reliability (ICC for absolute agreement = 0.57 [95% CI: 0.34 to 0.71]; p < 0.001) were present between CFR<sub>MRI</sub> and CFR<sub>PET</sub>. Bland–Altman analysis revealed a mean bias of  $-0.74 \pm 0.98$  for CFR. MRI demonstrated a tendency to underestimate CFR at both patient and vessel levels. Table 2 (the bottom row) lists the mean values of MRI and PET measurements of CFR. CFR<sub>MRI</sub> was significantly lower than CFR<sub>PET</sub> (1.81  $\pm$  0.62 vs. 2.55  $\pm$  1.09; p < 0.001). MBF<sub>MRI</sub> and MBF<sub>PET</sub> obtained during rest and stress showed only poor to moderate correlation (r = 0.26, p = 0.015 and r = 0.43, p = 0.019, respectively). Bland–Altman analysis showed a mean bias of - 0.85  $\pm$  0.48 mL/g/min and - 1.89  $\pm$  0.64 mL/g/min for rest and stress MBF, respectively.

Figure 4 shows the ROC curves of MRI perfusion imaging for detecting impaired CFR as defined by  $^{13}$ N-ammonia PET. CFR<sub>MRI</sub> displayed an area under the curve (AUC) of 0.847 (95% CI: 0.669 to

TABLE 1 Patient characteristics.

Characteristic	Total (n = 30)	Preserved CFR (n = 19)	Impaired CFR ( $n = 11$ )	<i>p</i> -value
Age (years)	54.4 ± 8.8	53.9 ± 9.5	55.3 ± 7.7	0.686
Female	13 (43.4)	8 (42.1)	5 (45.5)	1.000
BMI (kg/m²)	24.3 ± 2.6	23.6 ± 2.4	25.4 ± 2.7	0.074
Stress HR (bpm)	99.6 ± 13.1	101.3 ± 14.6	96.7 ± 9.7	0.369
Rest HR (bpm)	74.2 ± 9.6	74.2 ± 9.6	74.4 ± 9.9	0.956
SBP (mm Hg)	133.1 ± 12.8	130.8 ± 10.9	137.0 ± 15.2	0.208
DBP (mm Hg)	82.1 ± 9.3	81.9 ± 10.1	82.5 ± 8.3	0.857
Symptomatic status				0.637
Typical angina	13 (43.3)	7 (36.78)	6 (54.5)	
Atypical angina	9 (30)	6 (31.6)	3 (27.3)	
Asymptomatic	8 (26.7)	6 (31.6)	2 (18.2)	
Medication				
ACEI or ARB	5 (16.7)	3 (15.8)	2 (18.2)	1.000
Aspirin	13 (43.4)	8 (42.1)	5 (45.5)	1.000
Beta-blockers	10 (33.3)	5 (26.3)	5 (45.5)	0.425
CCB	10 (33.3)	5 (26.3)	5 (45.5)	0.425
Nitrates	7 (23.3)	2 (10.5)	5 (45.5)	0.068
Statins	17 (56.7)	10 (52.6)	7 (63.6)	0.708
Oral hypoglycemic agents	3 (10.0)	0 (0.0)	3 (27.2)	0.041
Laboratory values				
Total Cholesterol, mmol/L	4.55 ± 1.19	4.51 ± 0.86	4.60 ± 1.66	0.868
Triglyceride, mmol/L	1.18 ± 0.58	0.91 ± 0.40	$1.66 \pm 0.54$	< 0.001
HDL cholesterol, mmol/L	1.28 ± 0.43	1.33 ± 0.41	$1.20 \pm 0.47$	0.425
VLDL cholesterol, mmol/L	0.61 ± 0.24	0.55 ± 0.19	0.71 ± 0.30	0.081
LDL cholesterol, mmol/L	2.58 ± 0.90	2.60 ± 0.80	2.56 ± 1.09	0.918
WBC, 10 <sup>9</sup> /L	6.03 ± 1.84	5.82 ± 1.80	6.40 ± 1.95	0.417
PLT, 109/L	225.6 ± 54.4	224.4 ± 54.2	227.7 ± 57.4	0.874
Neutrophil, 10 <sup>9</sup> /L	3.77 ± 1.20	3.83 ± 1.30	3.65 ± 1.06	0.704
Monocyte, 10 <sup>9</sup> /L	$0.42 \pm 0.16$	$0.42 \pm 0.15$	$0.43 \pm 0.18$	0.957
Lymphocyte, 10 <sup>9</sup> /L	1.98 ± 0.78	1.88 ± 0.52	2.17 ± 1.10	0.418
Hemoglobin, g/dl	137.3 ± 13.9	137.5 ± 14.89	136.9 ± 12.68	0.909
RBC, 10 <sup>12</sup> /L	4.61 ± 0.53	4.65 ± 0.42	4.55 ± 0.69	0.626

<sup>\*</sup> Values are mean  $\pm$  SD or n (%).

ACEI, angiotensin-converting-enzyme inhibitors; ARB, angiotensin receptor blocker; BMI, body mass index; CCB, calcium-channel blocker; HDL, high-density lipoprotein; VLDL, very-low-density lipoprotein; DBP, diastolic blood pressure; SBP, systolic blood pressure.

0.952) and an optimal cutoff value of 1.57 (sensitivity: 72.73%; specificity: 89.47%). Figure 5 shows a 39-year-old symptomatic male in the impaired CFR group. First-pass MRI (Panel A) reveals uniform rest perfusion but diffuse mid-apical signal reduction under stress, consistent with microvascular dysfunction. Corresponding  $^{13}$ N-ammonia PET (Panel B) shows matching stress tracer uptake defects. Quantitative analysis (Panels C–E) demonstrates moderate agreement in global CFR (MRI: 1.20; PET: 1.48), aligning with the cohort's overall correlation (r=0.64), while stress MBF differs more notably (MRI: 1.12 vs. PET: 2.12 mL/g/min), reflecting the broader trend of larger MBF discrepancies. This case exemplifies the study's key findings: consistent CFR for CMD diagnosis despite variable absolute MBF.

# 3.4 Comorbidity subgroup analyses

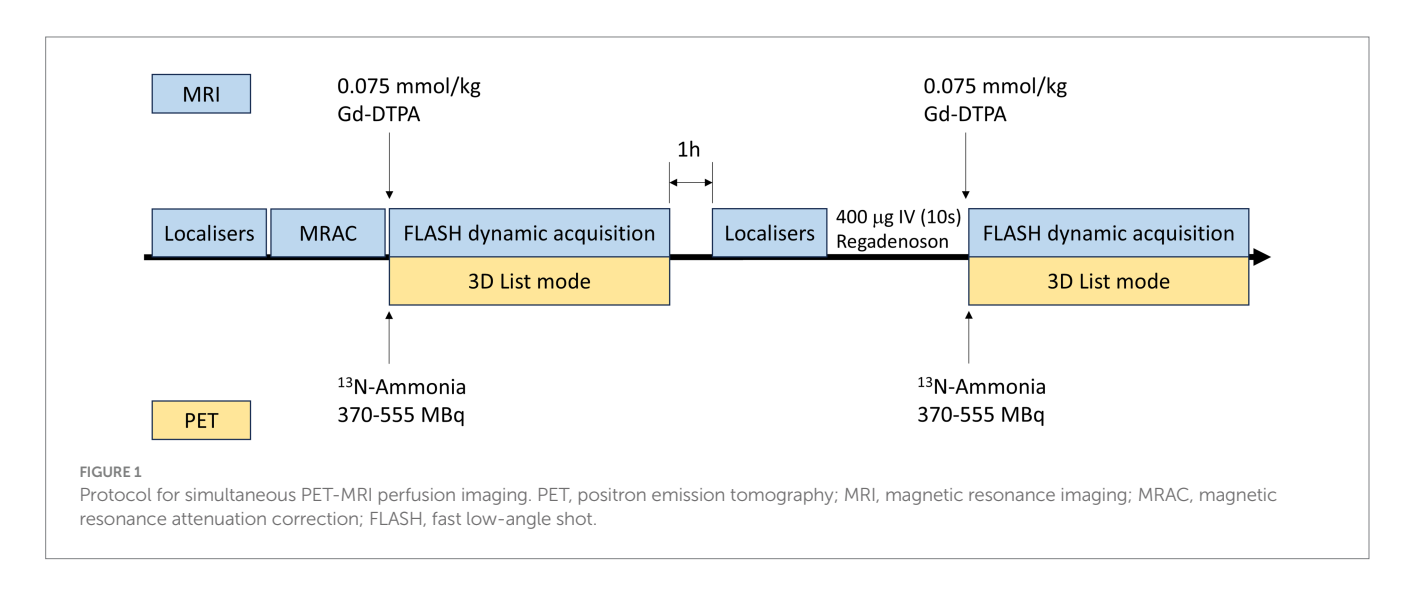
To further explore the impact of comorbidities, and given that diabetes was the only condition associated with a significant CFR difference (Table 3), we conducted subgroup analyses in patients with and without diabetes (Figures 6, 7). Despite the known microvascular alterations in diabetes, the overall correlation between MRI and PET for CFR persisted, though myocardial blood flow (MBF) measurements exhibited greater variability in diabetic patients—aligning with characteristics of diabetic microvascular dysfunction. Importantly, the diagnostic performance of MRI-derived CFR (using the established cutoff of 1.57 for CMD) remained robust across both

TABLE 2 Patient hemodynamic parameters.

Variables	MRI	<sup>13</sup> N-ammonia PET	p-value					
Left ventricular end-systolic volume (mL)	46.90 ± 10.78	36.72 ± 12.58	<0.001					
Left ventricular end-diastolic volume (mL)	117.28 $\pm$ 21.25 90.34 $\pm$ 30.63		<0.001					
Left ventricular ejection fraction (%)	60.76 ± 7.34	62.01 ± 8.74	0.501					
Global perfusion								
CFR	1.77 ± 0.49	2.56 ± 1.08	<0.001					
Regional perfusion								
CFR	1.81 ± 0.62	2.55 ± 1.09	<0.001					

<sup>\*</sup> Values are mean ± SD.

LV, left ventricle; PET, positron emission tomography; MRI, magnetic resonance imaging; CFR, coronary flow reserve.



subgroups. These results indicate that while diabetes influences microvascular perfusion (evident in MBF variability), it does not negate the core agreement between MRI and PET for evaluating global CFR, thus supporting the primary findings.

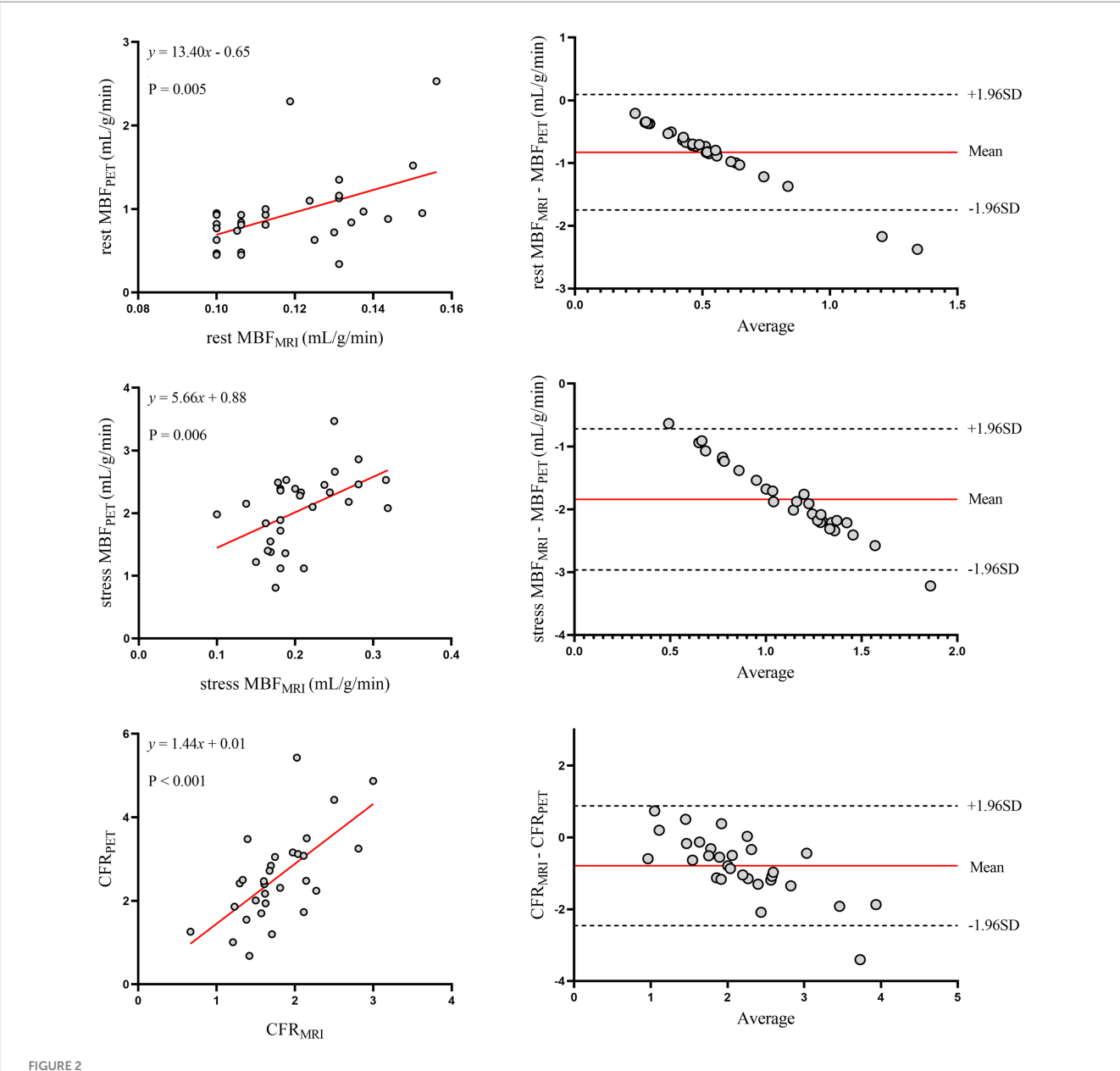
### 4 Discussion

The current study represents the largest investigation to date of the agreement between MRI and PET measurements of myocardial perfusion. In this study, the feasibility of simultaneous CFR quantification using hybrid PET-MRI scanner was confirmed in a cohort of patients with suspected CMD, setting the stage for a future clinical study to compare PET and MRI CFR values in suspected CMD. While consistency was only moderate with substantial variability, strong correlations and negligible bias were observed between the two methods for both global and regional myocardial perfusion. Thus, in clinical settings, MRI for quantifying myocardial perfusion is an attractive alternative to PET for CMD diagnosis.

PET is widely regarded as the non-invasive gold standard for MBF quantification (16). Despite its short half-life (9.96 min), <sup>13</sup>N-ammonia remains the gold standard perfusion tracer due to its balanced practicality and image quality—attributes amplified by short positron range and myocardial retention—and is ideally suited for validating novel real-time CMR perfusion techniques with automated quantification potential for clinical implementation (17, 18). Such a study could accelerate acceptance of CMR perfusion as a viable

alternative for MBF measurements, enabling broader adoption without the need for ionizing radiation and costly radiochemistry facilities. Additionally, it provides information on left ventricular function and viability, making CMR well-suited for non-invasive CMD evaluation.

CFR is a commonly used measure in the diagnosis of CMD. In our results, CFR values were generated within the normal ranges reported in the literature, both for MRI (19) and for PET (20, 21). Previous studies comparing quantitative CMR and PET myocardial perfusion were limited to patient cohorts, with substantial variability in study populations (i.e., typical angina patients vs. healthy volunteers), PET radiotracers used, CMR image acquisition techniques, and CMR field strength. Engblom et al. (14) showed a strong correlation for CFR values (r = 0.92, p < 0.001) quantified by PET and MRI. Qayyum et al. (22) reported that, on a global and vessel territorial basis, MRI results were strongly correlated with PET results for CFR (r = 0.89, p < 0.001). Pack et al. (23) studied 4 healthy volunteers with <sup>13</sup>N-ammonia PET and CMR perfusion imaging at 3-T and reported similar results. Morton et al. (12) compared quantitative CMR and PET myocardial perfusion in 41 patients with known or suspected CAD, finding strong correlations between CMR-and PET-derived MPRI (r = 0.75, p < 0.001) despite weak correlations in absolute perfusion values. These findings are consistent with our observations. In our data, there was good correlation between MRI-and PET-based CFR values (r = 0.64, p < 0.001). However, Kero et al. (24) shown that there was no significant correlation between MRI-and PET-derived CFR values (r = 0.08, p = 0.80), which in this case can be explained by physiological differences between MRI and PET.

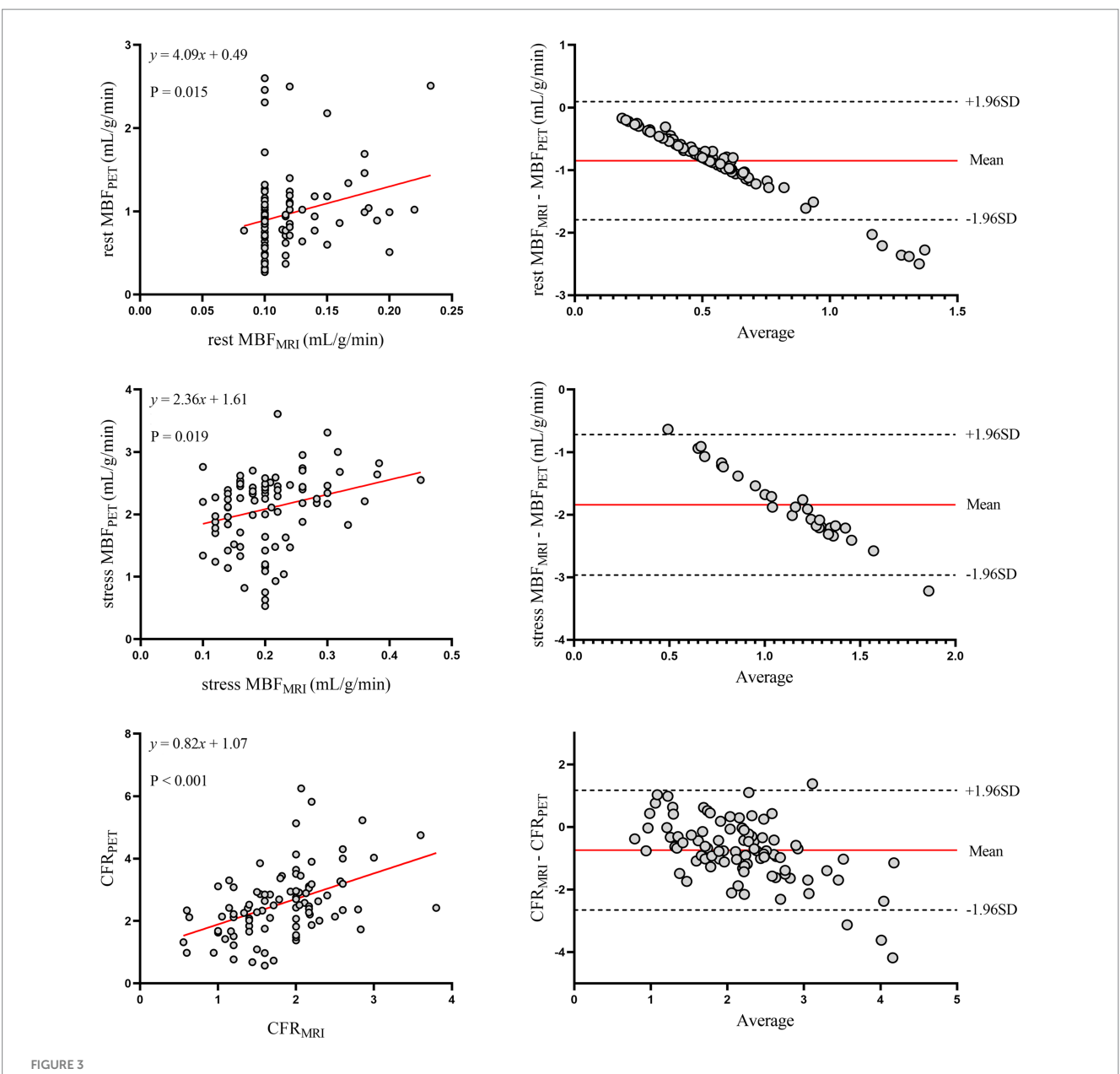


Global myocardial perfusion. Left panels display scatter plots and right panels show Bland–Altman plots comparing MRI and <sup>13</sup>N-ammonia PET measurements of MBF at rest (top), under stress (middle), and CFR (bottom) on a global basis. In the Bland–Altman plots, the solid red line indicates the mean bias, and the dashed black lines indicate +1.96SD and –1.96SD, respectively. PET, positron emission tomography; MRI, magnetic resonance imaging; MBF, myocardial blood flow; CFR, coronary flow reserve.

Accurately quantifying MBF with MRI remains challenging due to the non-linear relationship between signal intensity and gadolinium contrast concentration. Key sources of non-linearity and bias include spatial signal variations due to surface coil sensitivity profiles, incomplete saturation of magnetization during contrast agent bolus passage, T2\* decay from high contrast concentrations in the blood pool, and inherent non-linear signal responses resulting from saturation recovery dependent on imaging protocol parameters (25). In our study, a 0.075 mmol/kg dose of Gd-DTPA was administered, with no evidence of bolus peak flattening due to saturation effects observed. To avoid signal saturation effects, low contrast agent doses (0.05 mmol/kg) have been used in some studies (26, 27). Similarly, no evidence of bolus peak flattening due to saturation effects was observed.

If saturation effects are present but overlooked, myocardial perfusion results may be overestimated, which was not evident in our findings.

MRI and PET showed significant differences in left ventricular functional parameters, with MRI measuring larger end-diastolic volumes (117.28  $\pm$  21.25 mL vs. 90.34  $\pm$  30.63 mL, p < 0.001) and end-systolic volumes than PET, though ejection fractions were comparable (Table 2). Clinically, these discrepancies matter because left ventricular volumes are key for assessing cardiac remodeling and disease progression. MRI, with superior soft tissue resolution and breath-hold acquisition, likely provides more accurate volumetric data, while PET may underestimate volumes due to motion artifacts from free breathing or attenuation correction differences. For CMD patients, where subtle ventricular remodeling could relate to



Regional myocardial perfusion. Left panels display scatter plots and right panels show Bland–Altman plots comparing MRI and <sup>13</sup>N-ammonia PET measurements of MBF at rest (top), under stress (middle), and CFR (bottom) on a per-vessel basis. In the Bland–Altman plots, the solid red line indicates the mean bias, and the dashed black lines indicate +1.96SD and –1.96SD, respectively. PET, positron emission tomography; MRI, magnetic resonance imaging; MBF, myocardial blood flow; CFR, coronary flow reserve.

TABLE 3 Comparison of CFR between patients with and without hypertension, dyslipidemia, or diabetes.

Comorbidity	Hypertension		Dyslipidemia		Diabetes	
	With	Without	With	Without	With	Without
CFR	$2.24 \pm 0.76$	2.81 ± 1.24	2.44 ± 1.43	2.61 ± 0.93	1.79 ± 0.52	2.84 ± 1.10
p-value	0.154		0.692		0.015	

<sup>\*</sup> Values are mean ± SD. CFR, coronary flow reserve.

microvascular dysfunction, these differences highlight the need to interpret volume-based metrics cautiously when switching between modalities—MRI may be preferred for tracking structural changes, while PET remains valuable for perfusion-focused assessments.

Regarding characteristics of our study population, we have demonstrated that in 30 patients with suspected CMD undergoing myocardial perfusion PET, 36.7% had lower global CFR (< 2.0). The unique relationship between symptoms and impaired CFR highlighted

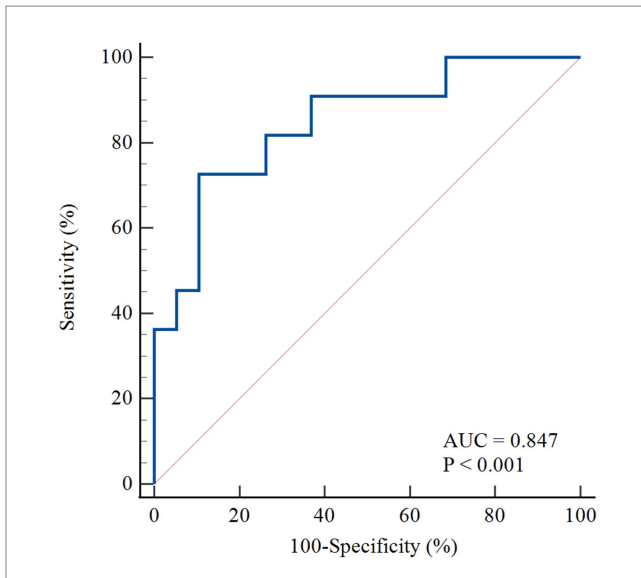
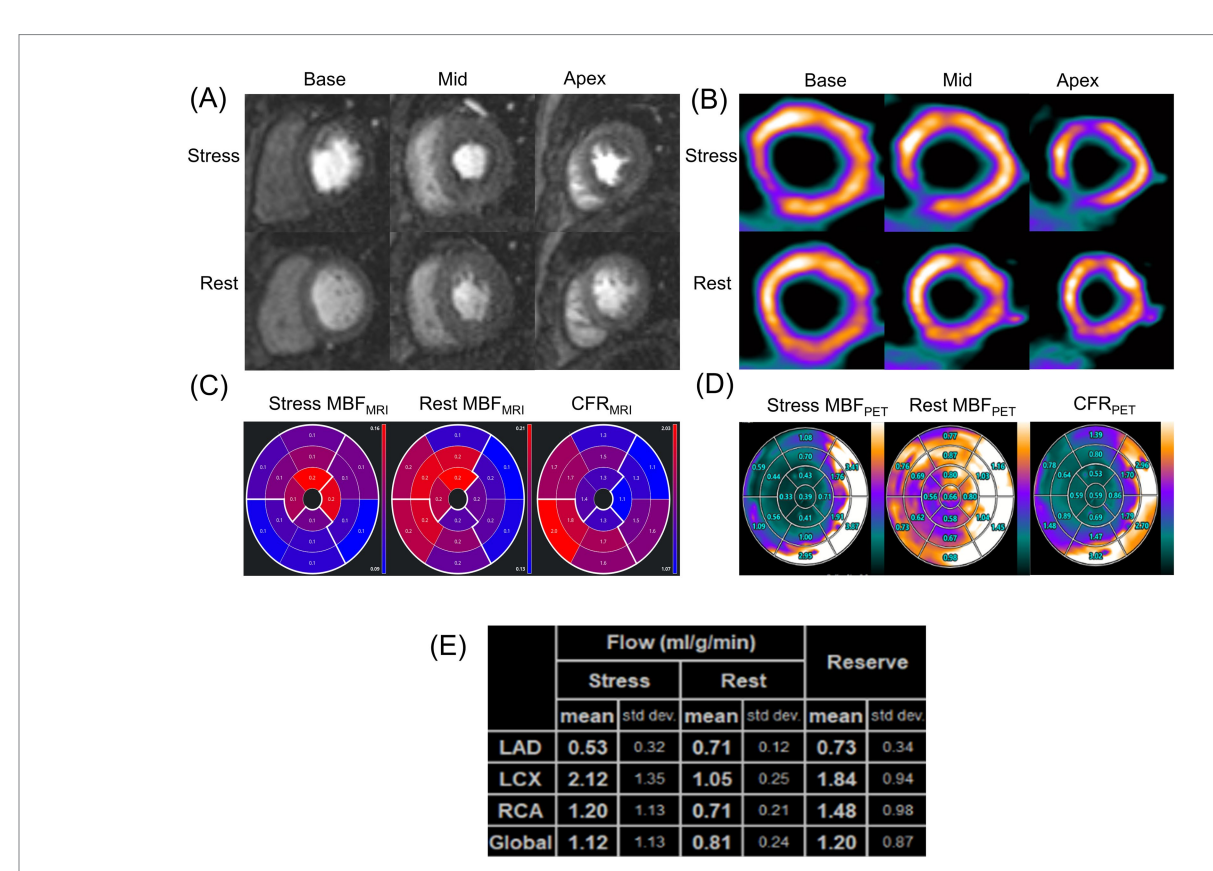


FIGURE 4
The ROC curve for the detection of abnormal perfusion. The ROC curve of MRI derived CFR for detecting abnormal perfusion defined as 13 N-ammonia PET-derived CFR < 2.0. AUC, area under the curve; ROC, receiver operating characteristic; PET, positron emission tomography; MRI, magnetic resonance imaging; MBF, myocardial blood flow; CFR, coronary flow reserve.

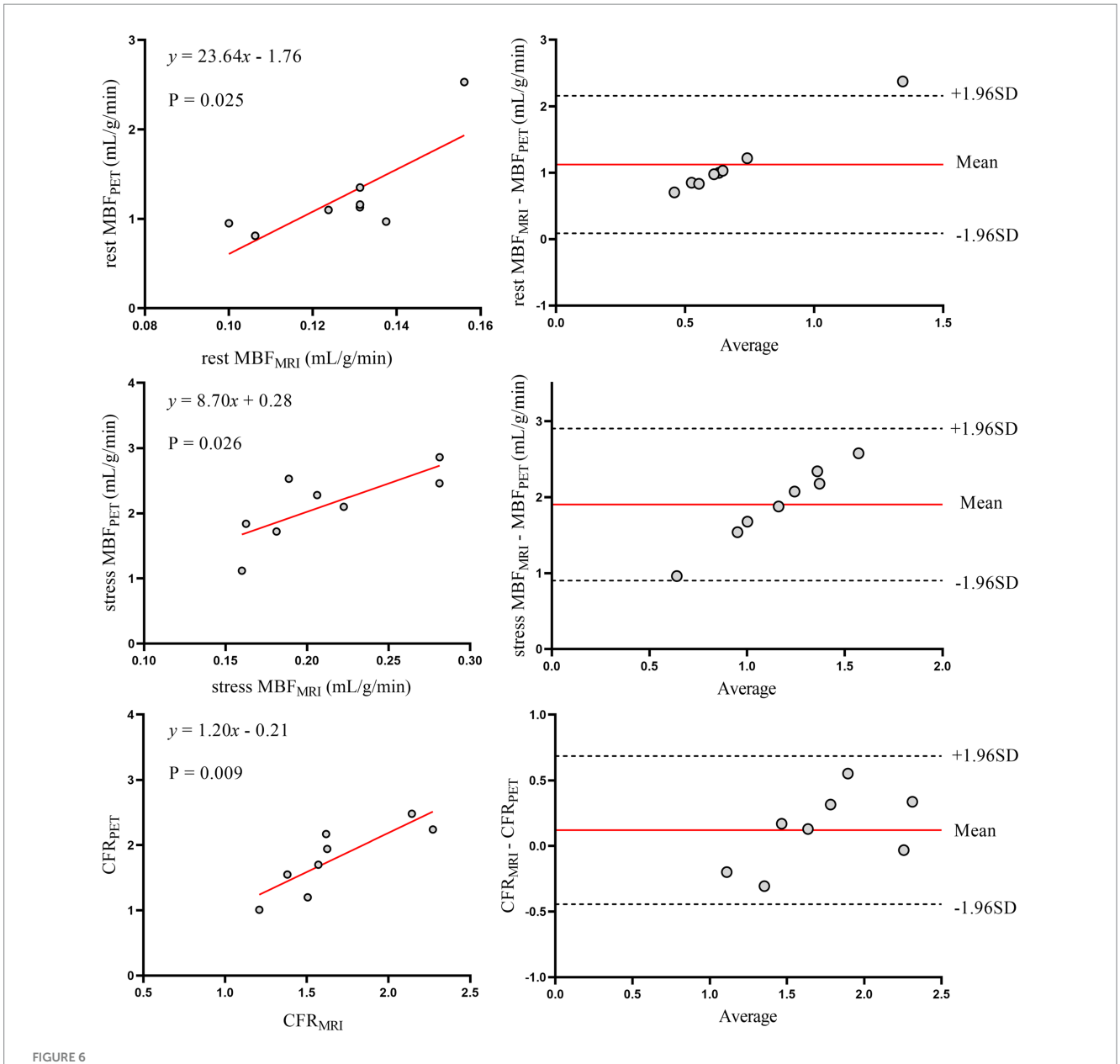
no statistical difference in symptomatic status between the two groups, with approximately 18.2% of the impaired CFR group being asymptomatic. Patients without obstructive coronary artery disease are often told their chest pain is noncardiac. As a result, further evaluation is frequently deferred, leading to missed opportunities to diagnose CMD and initiate treatments to reduce cardiovascular risk. Similar to previous findings (28), a more rapid MFR decline has been observed in diabetic patients compared to non-diabetic counterparts in the presence of significant obstructive epicardial disease. We further analyzed comorbidities. Only diabetes was linked to significant CFR differences (Table 3). Even so, diabetes did not break the core agreement between MRI and PET for global CFR. MBF measurements showed slightly more variability in diabetic patients. But the diagnostic value of MRI-derived CFR for CMD stayed strong in both diabetic and non-diabetic subgroups (Figures 6, 7). Given that diabetes-related differences did not nullify the primary findings on CFR agreement or diagnostic utility, additional model adjustments to correct for these confounding factors were not deemed necessary. Overall, implications for the diagnosis and management of CAD patients with these and other traditional cardiovascular risk factors for microvascular disease have been highlighted by this observation.

In this current study, MRI-derived CFR values underestimated PET values in CMD patients, particularly at higher values, and these findings are in keeping with previous clinical studies that compared



### FIGURE 5

A representative case of a symptomatic 39-year-old man in the impaired CFR group. (A) First-pass perfusion images at rest and stress. (B) <sup>13</sup>N-ammonia PET images at rest and stress. (C) MRI-derived quantification value of stress MBF (left), rest MBF (center) and, CFR (right). (D) Regadenoson-induced <sup>13</sup>N-ammonia PET-derived quantification value of stress MBF (left), rest MBF (center) and, CFR (right) in the 17-segment standard American Heart Association model and (E) based on the three major coronary territories. PET, positron emission tomography; MRI, magnetic resonance imaging; MBF, myocardial blood flow; CFR, coronary flow reserve.



Correlation and agreement of myocardial perfusion metrics (CFR, rest/stress MBF) between MRI and <sup>13</sup>N-ammonia PET in patients with diabetes mellitus. Left panels (top to bottom): scatter plots with linear regression for rest MBF, stress MBF, and CFR between MRI and PET in patients with diabetes. Right panels: Bland–Altman plots illustrating agreement, with solid red lines denoting mean bias and dashed lines representing 95% limits of agreement (LoA). PET, positron emission tomography; MRI, magnetic resonance imaging; MBF, myocardial blood flow; CFR, coronary flow reserve.

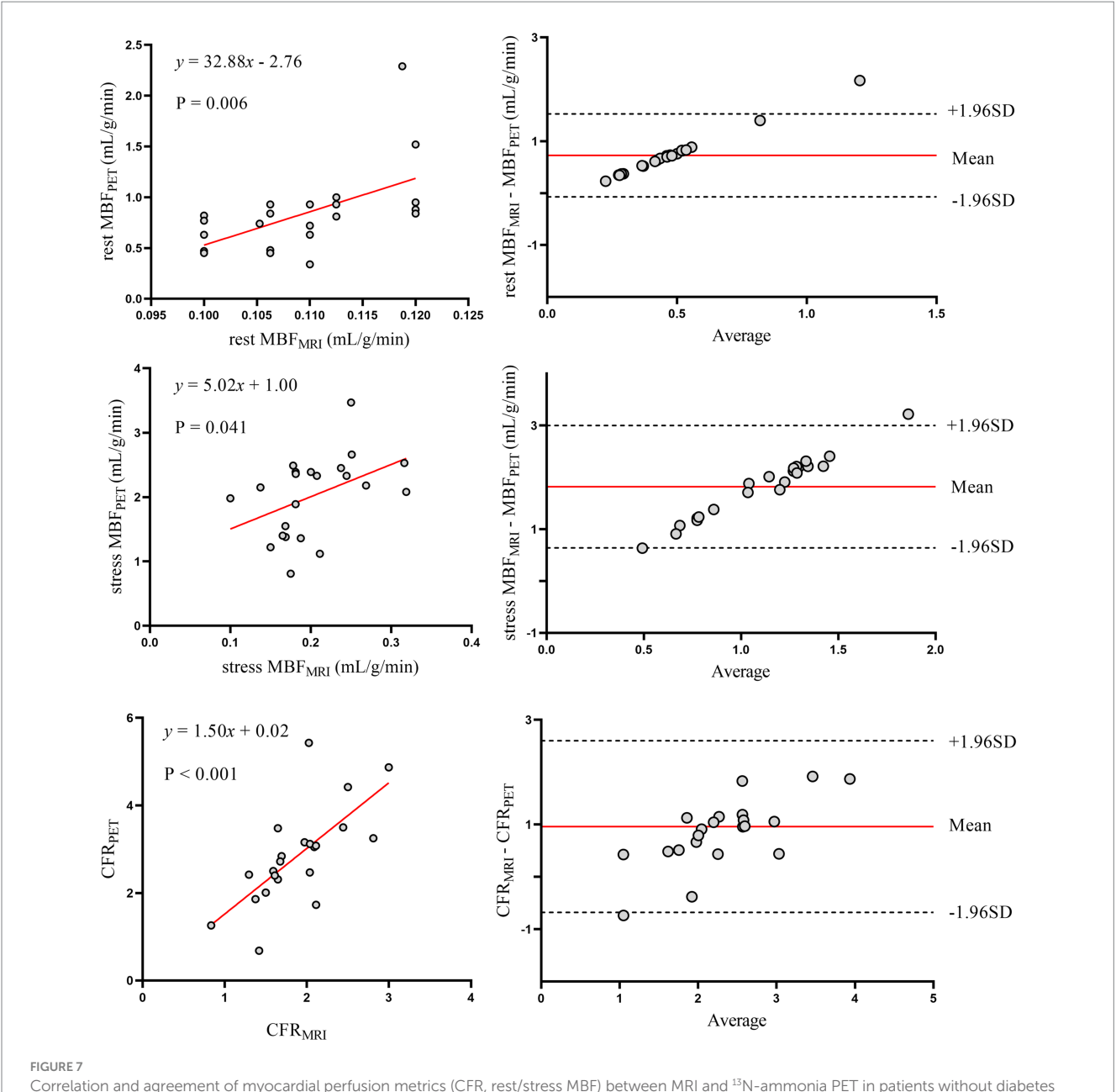
PET and CMR-derived CFR (11). There are several plausible reasons to explain the underestimation of CMR-derived MBF values observed in the phantom studies and the volunteer study. MRI signal intensity and gadolinium concentration demonstrate a non-linear relationship (26). This is primarily attributed to the kinetic properties of gadolinium-based contrast agents. The extraction fraction of gadolinium-based contrast agents decreases unpredictably from approximately 0.55 at rest with increasing flow rates, leading to underestimation of tissue response curves at higher flows and subsequent underestimation of CFR. PET MBF quantification avoids this limitation as the activity measured directly correlates with tracer concentration.

Figure 5's representative case validates the study's methodology and findings. It demonstrates simultaneous PET-MRI feasibility,

eliminating inter-scan variability to strengthen correlation reliability. The case visually confirms core results: CFR alignment and stress MBF discrepancies (mirroring cohort trends, likely due to contrast kinetics). Clinically, it links imaging findings to symptomatic CMD—diffuse stress defects without obstructive disease—bridging quantitative data and real-world diagnosis, reinforcing MRI's value for identifying microvascular dysfunction.

# 4.1 Study limitations

First, the study enrolled relatively small sample size. Nevertheless, this is the first study in patients and larger than previous



Correlation and agreement of myocardial perfusion metrics (CFR, rest/stress MBF) between MRI and <sup>13</sup>N-ammonia PET in patients without diabetes mellitus. Left panels (top to bottom): scatter plots with linear regression for rest MBF, stress MBF, and CFR between MRI and PET in patients without diabetes. Right panels: Bland–Altman plots for agreement. PET, positron emission tomography; MRI, magnetic resonance imaging; MBF, myocardial blood flow; CFR, coronary flow reserve.

volunteer-based studies. Second, respiratory control differences—MRI requiring breath-holds versus PET allowing free breathing—may introduce variability in MBF quantification. MRI breath-holds minimize motion artifacts, improving spatial resolution for regional MBF analysis, but brief breath-holding could transiently alter hemodynamics (e.g., subtle heart rate changes) that affect stress-induced hyperemia. In contrast, PET's free-breathing approach avoids such transient physiological shifts but may introduce motion-related blurring, particularly in inferior myocardial segments, potentially diluting regional MBF accuracy. These differences likely contribute to the observed discrepancies in MBF between modalities, as motion artifacts and physiological perturbations disproportionately affect absolute perfusion values. Third, while PET MBF and CFR analysis are

performed robustly and automatically within minutes using commercial software, MRI analysis remains time-consuming, operator-dependent, and error-prone. Finally, CFR interpretation should be exercised with caution when assigning myocardial segments to coronary artery territories based on common vascular distribution patterns. However, interindividual variability in coronary anatomy may render such assumptions potentially inaccurate.

# 5 Conclusion

The  $CFR_{PET}$  and  $CFR_{MRI}$  seem to predict CMD equally well and accurately. However, in patients, the absolute perfusion values from

PET and MRI are only modestly correlated, indicating the need for further refinement of quantitative techniques.

# Data availability statement

The original contributions presented in the study are included in the article/supplementary material, further inquiries can be directed to the corresponding authors.

### Ethics statement

The studies involving humans were approved by Ethics Committee of Anhui Provincial Hospital. The studies were conducted in accordance with the local legislation and institutional requirements. The participants provided their written informed consent to participate in this study. Written informed consent was obtained from the individual(s) for the publication of any potentially identifiable images or data included in this article.

# **Author contributions**

RW: Writing – original draft, Writing – review & editing. QX: Data curation, Writing – review & editing. BP: Writing – review & editing. MN: Formal analysis, Writing – review & editing. XZ: Methodology, Writing – review & editing. XM: Validation, Writing – review & editing. ZW: Methodology, Writing – review & editing. XiW: Investigation, Writing – review & editing. DL: Conceptualization, Writing – review & editing. XuW: Funding acquisition, Resources, Supervision, Writing – review & editing.

# **Funding**

The author(s) declare that financial support was received for the research and/or publication of this article. This work was supported

by USTC Research Funds of the Double First-Class Initiative (YD9110002055 to XW) and Regional Development Joint Fund Integration Project (U22A6008 to XW).

# Acknowledgments

The author thanks the staff of the Department of Nuclear Medicine, the First Affiliated Hospital of the University of Science and Technology of China for their support of this research.

# Conflict of interest

The authors declare that the research was conducted in the absence of any commercial or financial relationships that could be construed as a potential conflict of interest.

# Generative AI statement

The authors declare that no Gen AI was used in the creation of this manuscript.

Any alternative text (alt text) provided alongside figures in this article has been generated by Frontiers with the support of artificial intelligence and reasonable efforts have been made to ensure accuracy, including review by the authors wherever possible. If you identify any issues, please contact us.

# Publisher's note

All claims expressed in this article are solely those of the authors and do not necessarily represent those of their affiliated organizations, or those of the publisher, the editors and the reviewers. Any product that may be evaluated in this article, or claim that may be made by its manufacturer, is not guaranteed or endorsed by the publisher.

### References

- 1. Pepine CJ, Anderson RD, Sharaf BL, Reis SE, Smith KM, Handberg EM, et al. Coronary microvascular reactivity to adenosine predicts adverse outcome in women evaluated for suspected ischemia results from the National Heart, lung and blood institute wise (women's ischemia syndrome evaluation) study. *J Am Coll Cardiol.* (2010) 55:2825–32. doi: 10.1016/j.jacc.2010.01.054
- 2. Crea F, Montone RA, Rinaldi R. Pathophysiology of coronary microvascular dysfunction. Circ J. (2022) 86:1319–28. doi: 10.1253/circj.CJ-21-0848
- 3. Marinescu MA, Löffler AI, Ouellette M, Smith L, Kramer CM, Bourque JM. Coronary microvascular dysfunction, microvascular angina, and treatment strategies. *JACC Cardiovasc Imaging*. (2015) 8:210–20. doi: 10.1016/j.jcmg.2014.12.008
- 4. Rahman H, Corcoran D, Aetesam-Ur-Rahman M, Hoole SP, Berry C, Perera D. Diagnosis of patients with angina and non-obstructive coronary disease in the catheter laboratory. *Heart*. (2019) 105:1536–42. doi: 10.1136/heartjnl-2019-315042
- 5. Schindler TH, Fearon WF, Pelletier-Galarneau M, Ambrosio G, Sechtem U, Ruddy TD, et al. Myocardial perfusion pet for the detection and reporting of coronary microvascular dysfunction: a Jacc: cardiovascular imaging expert panel statement. *JACC Cardiovasc Imaging*. (2023) 16:536–48. doi: 10.1016/j.jcmg.2022.12.015
- 6. Schindler TH, Dilsizian V. Coronary microvascular dysfunction: clinical considerations and noninvasive diagnosis. *JACC Cardiovasc Imaging.* (2020) 13:140–55. doi: 10.1016/j.jcmg.2018.11.036
- 7. Nazir MS, Gould SM, Milidonis X, Reyes E, Ismail TF, Neji R, et al. Simultaneous (13) N-Ammonia and gadolinium first-pass myocardial perfusion with quantitative

- hybrid pet-Mr imaging: a phantom and clinical feasibility study. Eur J Hybrid Imaging. (2019) 3:15. doi: 10.1186/s41824-019-0062-6
- 8. Sakuma H, Ishida M. Advances in myocardial perfusion Mr imaging: physiological implications, the importance of quantitative analysis, and impact on patient Care in Coronary Artery Disease. *Magn Reson Med Sci.* (2022) 21:195–211. doi: 10.2463/mrms.rev.2021-0033
- 9. Buckert D, Witzel S, Steinacker JM, Rottbauer W, Bernhardt P. Comparing cardiac magnetic resonance–guided versus angiography-guided treatment of patients with stable coronary artery disease: results from a prospective randomized controlled trial. *JACC Cardiovasc Imaging*. (2018) 11:987–96. doi: 10.1016/j.jcmg.2018. 05.007
- 10. Mygind ND, Pena A, Mide Michelsen M, Ali Qayyum A, Frestad D, Emil Christensen T, et al. Myocardial first pass perfusion assessed by cardiac magnetic resonance and coronary microvascular dysfunction in women with angina and no obstructive coronary artery disease. Scand J Clin Lab Invest. (2019) 79:238–46. doi: 10.1080/00365513.2019.1587670
- 11. Everaars H, van Diemen PA, Bom MJ, Schumacher SP, de Winter RW, van de Ven PM, et al. Comparison between quantitative cardiac magnetic resonance perfusion imaging and [150]H2o positron emission tomography. *Eur J Nucl Med Mol Imaging*. (2020) 47:1688–97. doi: 10.1007/s00259-019-04641-9
- 12. Morton G, Chiribiri A, Ishida M, Hussain ST, Schuster A, Indermuehle A, et al. Quantification of absolute myocardial perfusion in patients with coronary artery disease:

comparison between cardiovascular magnetic resonance and positron emission tomography. *J Am Coll Cardiol.* (2012) 60:1546–55. doi: 10.1016/j.jacc.2012.05.052

- 13. Akil S, Hedeer F, Carlsson M, Arheden H, Oddstig J, Hindorf C, et al. Qualitative assessments of myocardial ischemia by cardiac Mri and coronary stenosis by invasive coronary angiography in relation to quantitative perfusion by positron emission tomography in patients with known or suspected stable coronary artery disease. *J Nucl Cardiol.* (2020) 27:2351–9. doi: 10.1007/s12350-018-01555-1
- 14. Engblom H, Xue H, Akil S, Carlsson M, Hindorf C, Oddstig J, et al. Fully quantitative cardiovascular magnetic resonance myocardial perfusion ready for clinical use: a comparison between cardiovascular magnetic resonance imaging and positron emission tomography. *J Cardiovasc Magn Reson.* (2017) 19:78. doi: 10.1186/s12968-017-0388-9
- 15. Whelton PK, Carey RM, Mancia G, Kreutz R, Bundy JD, Williams B. Harmonization of the American College of Cardiology/American Heart Association and European Society of Cardiology/European Society of Hypertension Blood Pressure/hypertension guidelines: comparisons, reflections, and recommendations. *Circulation*. (2022) 146:868–77. doi: 10.1161/CIRCULATIONAHA.121.054602
- 16. Driessen RS, Raijmakers PG, Stuijfzand WJ, Knaapen P. Myocardial perfusion imaging with pet. *Int J Cardiovasc Imaging*. (2017) 33:1021–31. doi: 10.1007/s10554-017-1084-4
- 17. Maddahi J, Packard RR. Cardiac pet perfusion tracers: current status and future directions. Semin Nucl Med. (2014) 44:333–43. doi: 10.1053/j.semnuclmed.2014.06.011
- 18. Kellman P, Hansen MS, Nielles-Vallespin S, Nickander J, Themudo R, Ugander M, et al. Myocardial perfusion cardiovascular magnetic resonance: optimized dual sequence and reconstruction for quantification. *J Cardiovasc Magn Reson.* (2017) 19:43. doi: 10.1186/s12968-017-0355-5
- 19. Brown LAE, Onciul SC, Broadbent DA, Johnson K, Fent GJ, Foley JRJ, et al. Fully automated, inline quantification of myocardial blood flow with cardiovascular magnetic resonance: repeatability of measurements in healthy subjects. *J Cardiovasc Magn Reson*. (2018) 20:48. doi: 10.1186/s12968-018-0462-y
- 20. Chang CY, Hung GU, Hsu B, Yang BH, Chang CW, Hu LH, et al. Simplified quantification of (13) N-Ammonia pet myocardial blood flow: a comparative study with

- the standard compartment model to facilitate clinical use. J Nucl Cardiol. (2020) 27:819-28. doi: 10.1007/s12350-018-1450-1
- 21. Miura S, Naya M, Kumamaru H, Ando A, Miyazaki C, Yamashita T. Prognostic value of modified coronary flow capacity by (13) N-Ammonia myocardial perfusion positron emission tomography in patients without obstructive coronary arteries. *J Cardiol.* (2022) 79:247–56. doi: 10.1016/j.jjcc.2021.09.001
- 22. Qayyum AA, Hasbak P, Larsson HBW, Christensen TE, Ghotbi AA, Mathiasen AB, et al. Quantification of myocardial perfusion using cardiac magnetic resonance imaging correlates significantly to Rubidium-82 positron emission tomography in patients with severe coronary artery disease: a preliminary study. *Eur J Radiol.* (2014) 83:1120–8. doi: 10.1016/j.ejrad.2014.04.004
- 23. Pack NA, DiBella EVR, Rust TC, Kadrmas DJ, McGann CJ, Butterfield R, et al. Estimating myocardial perfusion from dynamic contrast-enhanced cmr with a model-independent deconvolution method. *J Cardiovasc Magn Reson.* (2008) 10:52. doi: 10.1186/1532-429X-10-52
- 24. Kero T, Johansson E, Engström M, Eggers KM, Johansson L, Ahlström H, et al. Evaluation of quantitative Cmr perfusion imaging by comparison with simultaneous (15) O-water-pet. *J Nucl Cardiol*. (2021) 28:1252–66. doi: 10.1007/s12350-019-01810-z
- 25. Kellman P, Aletras AH, Hsu L-y, McVeigh ER, Arai AE. T measurement during first-pass contrast-enhanced cardiac perfusion imaging. *Magn Reson Med.* (2006) 56:1132–4. doi: 10.1002/mrm.21061
- 26. Jerosch-Herold M. Quantification of myocardial perfusion by cardiovascular magnetic resonance. *J Cardiovasc Magn Reson.* (2010) 12:57. doi: 10.1186/1532-429x-12-57
- 27. Hsu LY, Kellman P, Arai AE. Nonlinear myocardial signal intensity correction improves quantification of contrast-enhanced first-pass Mr perfusion in humans. *J Magn Reson Imaging*. (2008) 27:793–801. doi: 10.1002/jmri.21286
- 28. Wu KY, Timmerman NP, McPhedran R, Hossain A, Beanlands RSB, Chong AY, et al. Differential association of Daibetes mellitus and female sex with impaired myocardial flaw reserve across the spectrum of epicardial coronary disease. *Eur Heart J Cardiovasc Imaging*. (2020) 21:576–84. doi: 10.1093/ehjci/jez163